Composites Part B 215 (2021) 108770

Contents lists available at ScienceDirect

Composites Part B

journal homepage: www.elsevier.com/locate/compositesb

Dihydromyricetin modification of boron nitride micro-sheets and construction of multilayer thermal conduction pathways in glass fiber reinforced epoxy composites

Hua Xiao [1], Fang Chen [1], Ze Ping Zhang [**], Min Zhi Rong [***], Ming Qiu Zhang [*]

Key Laboratory for Polymeric Composite and Functional Materials of Ministry of Education, GD HPPC Lab, School of Chemistry, Sun Yat-sen University, Guangzhou, 510275, PR China

ARTICLE INFO

Keywords:
A. polymer-matrix composites (PMCs)
B. Electrical properties
B. Thermal properties
B. Mechanical properties

ABSTRACT

In this paper, a novel non-covalent treatment method for the micron-sheets of inert hexagonal boron nitride (h-BN) was proposed by using natural flavonoid dihydromyricetin as modifier. The modified micro-sheets were further applied to fabricate thermally conductive glass fiber cloth reinforced epoxy (GFREP) composites. Specifically, the mixture of high concentration h-BN, acrylate copolymer and epoxy monomers were firstly coated on glass fiber cloth (GFC) to construct in-plane thermally conductive layer, and reduce the interfacial heat resistance between GFC and epoxy matrix. Afterwards, lower concentration h-BN was compounded with epoxy matrix, which provided through-plane thermal conductive paths and avoided excessive deterioration of mechanical properties. The produced GFREP composite exhibited high tensile strength retention (78.1%), excellent in-plane (2.36 W m^{-1} K^{-1}) and through-plane (0.76 W m^{-1} K^{-1}) thermal conductivity at 29.6 wt% h-BN content. This study offered an efficient way to develop high-performance GFREP composites with prominent thermal conductivity for integrated circuit packaging applications.

1. Introduction

Printed circuit boards (PCBs) have played an important role in supporting electronic components and heat dissipation [1]. Nowadays, with the development of electronic components towards high integration and miniaturization, the power density per unit mass or volume increases greatly. Large amounts of heat have to be generated and accumulated during service, leading to shortening of service life, deterioration of performance, and even burning out the electronic components directly [2–4]. Therefore, improved heat dissipation is highly desired in this case.

The insulating polymer composite substrate in PCBs used to be glass fiber reinforced epoxy, polyimide, phenolic resin, polyester, and bismaleimide [5]. Comparatively, glass fiber cloth (GFC) reinforced epoxy (GFREP) is mostly applied owing to its excellent mechanical and adhesion properties, good electrical insulation, low cost and easy processing [6]. Nevertheless, thermal conductivity (TC) of GFREP is rather low (0.2–0.3 W m^{-1} K^{-1} [7]), which fails to meet the increasing requirement for high heat dissipation. In recent years, various kinds of high thermal conductive inorganic ceramic fillers (e.g., hexagonal boron nitride (h-BN), alumina (Al_2O_3)) were incorporated into the epoxy matrix for establishment of efficient thermally conductive pathways in hopes of raising TC value of GFREP [6,8]. The research outcomes indicated that h-BN is rather attractive not only because of its high TC (about 250–600 W m^{-1} K^{-1} along the basal plane) [9,10] but also because of its superior electrical insulation and dielectric properties.

In general, increasing the content of thermally conductive fillers benefits formation of more thermal conduction paths in composite materials, but the high loading often reduces mechanical properties as a result of insufficient interfacial interaction [11,12]. With respect to the GFREP for commercial FR-4 (i.e., Flame Retardant Type 4) substrate, the weight fraction of glass fiber (e.g., type 1080) is about 30%. When a lot of particulate fillers (typically more than 50 wt%) were introduced to construct efficient thermal conduction paths, the content of matrix resin

* Corresponding author.
** Corresponding author.
*** Corresponding author.
E-mail addresses: zhangzp8@mail.sysu.edu.cn (Z.P. Zhang), cesrmz@mail.sysu.edu.cn (M.Z. Rong), ceszmq@mail.sysu.edu.cn (M.Q. Zhang).
[1] These authors contributed equally to this work.

https://doi.org/10.1016/j.compositesb.2021.108770
Received 10 January 2021; Received in revised form 14 February 2021; Accepted 5 March 2021
Available online 17 March 2021

would be too low to bond the reinforcement fabric and fillers simultaneously. Meanwhile, weight fraction of glass fibers in thermal conductive GFREP is generally less than that in common GFREP. Clearly, it is a challenge to achieve high TC and decent mechanical strength under the circumstances.

Herein, a facile and novel approach is proposed to tackle the issue. First, dihydromyricetin (DMY) is employed to functionalize inert h-BN micron platelets, which are difficult to be directly modified with general coupling agents (Fig. 1). Unlike the surface treatment agents including amino [13–16], alkali [17,18], acid [19,20], sodium cholate [21,22], polydopamine [23] and long-chain fatty amine [24], DMY, a physical modifier, is an abundant and cheap natural flavonoid complex with aromatic benzene ring coupling structure. Its molecular structure should have strong affinity for the basal plane of h-BN sheets by forming large π-bond conjugation (Fig. 1a). Secondly, since TC value of glass fiber cloth is generally too low to facilitate the transport of heat in composite, if GFC is imparted with TC in advance by coating DMY treated h-BN to construct in-plane thermally conductive layer (Fig. 1b), and then impregnated with the matrix resin containing fewer h-BN for formation of through-plane thermal conductive paths, we may obtain a GFREP with high TC at relatively lower content of h-BN. In this context, the negative influence of high particulate fillers loading on mechanical properties of the composite would be minimized.

To this end, epoxy, acrylate copolymer resin (ACR) binder and high concentration modified h-BN sheets are well mixed and coated on the surface of GFC to yield GFC@xA (refer to Fig. 1c, x denotes coating times, and A stands for acrylate copolymer resin). Afterwards, the GFC@xA is infiltrated by the epoxy monomers containing lower content h-BN so as to build up through-plane thermal conduction paths in the composite.

The physical and chemical properties of DMY-modified h-BN (h-BN@DMY) and thermally conductive GFREP are carefully analyzed in the following, and the relationship between structure and properties is also discussed. It is hoped that the results will provide a new idea for increasing the practicality of thermally conductive GFREP.

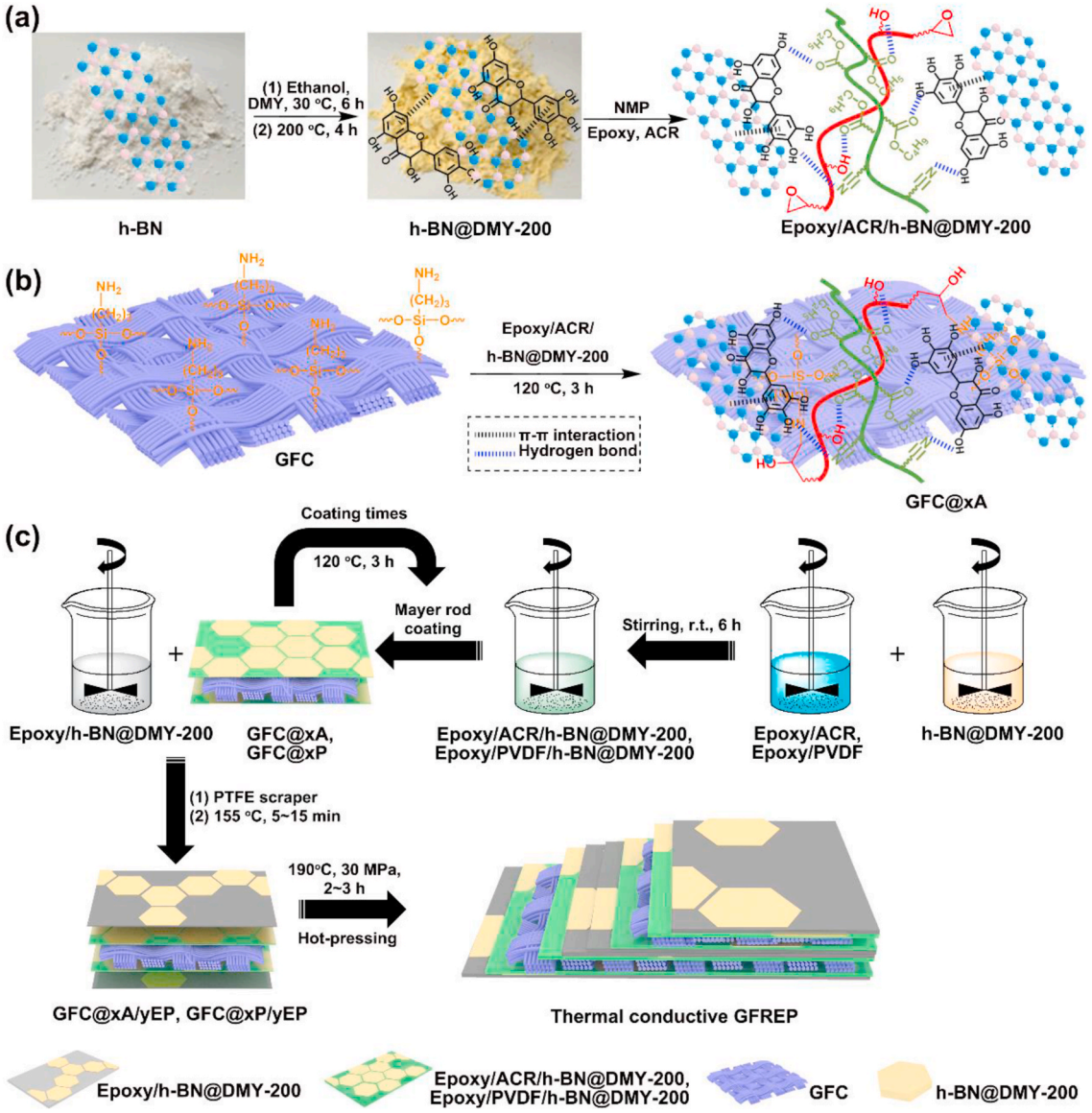

Fig. 1. (a) Synthesis of the materials. (b) Fabrication of GFC@xA; (c) Fabrication of the thermally conductive GFREP. (Note: h-BN@DMY-200: h-BN@DMY treated at 200 °C; ACR: acrylate copolymer resin; PVDF: polyvinylidene fluoride; GFC@xA: GFC coated with epoxy/ACR/h-BN@DMY-200 for *x* times; GFC@xP: GFC coated with epoxy/PVDF/h-BN@DMY-200 for *x* times; *y*: percentage of h-BN@DMY-200 °C in the epoxy based dip coating solution.)

2. Experimental

2.1. Materials

DMY (98%) was supplied by Xi'an Natural Field Biological Technology Co., Ltd., Xi'an, China. h-BN (99%, lateral size: 2–4 μm, thickness: 200–300 nm) was purchased from Dandong Rijin Technology Co., Ltd., Dandong, China. ACR (SG-708-6, M_n = 566946 g mol^{-1}, T_g = ~10 °C, acid value = 9 mg KOH g^{-1}) was obtained from Nagase ChemteX Co., Japan. Bromo-bisphenol A epoxy resin (DER 530A80, epoxy equivalent = 425–440 g eq^{-1}) was provided by Dow Inc., Midland, USA. Dicyandiamide (99%, DCD) and 2-methylimidazole (99%, 2-MI) were purchased from Aladdin Biochemical Technology Co., Ltd., Shanghai, China. PVDF powder (HSV900, T_g = 39 °C, T_m = ~164 °C) was obtained from ARKEMA, Paris, France. Electronic grade glass fiber cloth 1080 modified with 3-aminopropyltriethoxysilane (KH550) (Table S1) was supplied by Honghe Electronic Materials Technology Co., Ltd., Shanghai, China. All the other reagents were purchased from Guangzhou Chemical Reagent Factory and used as received.

2.2. Preparation of dihydromyricetin-modified h-BN (h-BN@DMY)

Typically, 100 g h-BN powders were firstly dispersed in 1 L ethanol in a glass bottle, and then 50 g of DMY was added. After stirring for 6 h at 30 °C, the reaction mixture was filtered, washed with ethanol and vacuum dried at 65 °C to obtain the pale-yellow powders of h-BN@DMY. For improving thermal stability, h-BN@DMY was further heat-treated in vacuum at 200 °C for 4 h, marked as h-BN@DMY-200.

2.3. Fabrication of the GFC coated with epoxy/ACR/h-BN@DMY-200 or epoxy/PVDF/h-BN@DMY-200

The mixture of DCD (3.616 g) and 2-MI (0.0826 g) with molar ratio of 4/1 was dissolved in 36.9 mL N,*N*-dimethylformamide (DMF), followed by adding 161.432 g bromo-bisphenol A epoxy resin DER 530A80 and stirring at room temperature to obtain the epoxy/hardener mixture solution, marked as 530A80/DCD/2-MI (solid content = 81.74%).

Meanwhile, 122.4 g h-BN@DMY-200 was dispersed in 400 mL N-methyl pyrrolidone (NMP) under mechanical stirring and ultrasonication. Then, 13.6 g ACR and 16.64 g 530A80/DCD/2-MI mixture solution (containing 13.74 g epoxy resin) were added into the h-BN dispersing solution (mass ratio of h-BN to resin = 4.5/1). Afterwards, the mixture was stirred at room temperature for 12 h to obtain uniformly dispersed coating solution with a concentration of 0.37 g mL^{-1}.

Subsequently, the coating solution was applied on both sides of GFC by a 200 μm Mayer rod, which was then dried at 120 °C for 3 h before the next coating. By controlling the daubing times (1–5), the modified GFC with different contents of h-BN were obtained and labeled as GFC@xA (x and A represent the coating time and polymer binder ACR, respectively). When ACR was replaced by PVDF, the reference sample GFC@xP was fabricated.

2.4. Fabrication of thermally conductive GFREP

Typically, a certain proportion of h-BN@DMY-200 (i.e., 0 wt%, 5 wt%, 10 wt%, 15 wt%, and 20 wt%) was firstly added to the 530A80/DCD/2-MI mixture solution. Then, GFC@xA was impregnated with the mixed solution through scraping with a polytetrafluoroethylene (PTFE) scraper, and then dried at 155 °C for 5–15 min to obtain the semi-curable sheets GFC@xA/yEP. Moreover, semi-curable GFC/0EP and GFC@xP/0EP sheets were prepared as references following the same procedures. Afterwards, two pieces of the same semi-curable sheets were overlapped and hot-pressed by a plate vulcanizer at 190 °C under 15–30 MPa for 2–3 h to obtain the thermally conductive GFREP.

The control composite containing unmodified h-BN, GFC@1A/20EP-ref, was fabricated following the same procedures as those applied to GFC@1A/20EP.

2.5. Characterization

Fourier transform infrared spectra (FTIR, Thermo Nicolet, Madison, USA) were recorded on a Bruker Tensor 27 from 400 to 4000 cm^{-1}. Proton nuclear magnetic resonance (^{1}H NMR) and carbon-13 nuclear magnetic resonance (^{13}C NMR) spectra were measured by an AVANCE III 400 MHz (400 MHz, Bruker, Karlsruhe, Germany) with chloroform-d as solvent. Wide angle X-ray diffraction (XRD) patterns were recorded by a D-MAX 2200 VPC X-ray diffractometer (Rigaku, Tokyo, Japan) with Cu-K$_\alpha$ (λ = 1.54 Å) radiation. Morphologies and microstructures of the composites were characterized by a Hitachi S4800 scanning electron microscopy (SEM, Hitachi, Tokyo, Japan) equipped with an energy dispersive X-ray spectroscopy (EDS) detector (IXRF). The tensile tests were carried out using a CMT6103 electronic universal testing machine (SANS, Shenzhen, China). Differential scanning calorimetry (DSC) measurements were performed with a TA DSC-Q10 (TA Instruments, New Castle, USA) in N_2 atmosphere at a heating rate of 10 °C min^{-1}. Dynamic mechanical analysis (DMA) was recorded with a 01 db Metravib DMA25 (ACOEM, Lyon, France) at a heating rate of 3 °C min^{-1} from room temperature to 200 °C. Water contact angle was measured with a K12 surface tension meter (Krüss, Hamburg, Germany) at ambient temperature. Five kinds of liquids (i.e., ethylene glycol, benzyl alcohol, water, ethanol and formamide) were applied to calculate the surface free energies. Tensile tests were performed using a CMT6103 electronic universal testing machine (SANS, Shenzhen, China) at 50 mm min^{-1}. The volume resistivity and surface resistivity were determined by a 4339B high resistance meters (Agilent, California, USA) at a voltage of 500 V and a charge time of 60 s.

Thermal gravimetric analysis (TGA) was recorded by a TG-Q50 instrument (TA Instruments, New Castle, USA) at a heating rate of 10 °C min^{-1} from 50 to 800 °C in an air stream with a flow rate of 40 ml min^{-1}. The BN content was estimated from:

$$\text{BN content} = (m_{R800}\text{-}m_{GFC})/m_o \times 100\% \quad (1)$$

where m_{R800} is the residual mass at 800 °C, m_{GFC} is the mass of GFC calculated from mass per unit area (46.8 g m^{-2}) and area of the tested sample, m_o is the sample mass.

The overall thermal conductivity (k_o) of the composites was characterized by a steady state heat flow thermal conductivity tester TIM LW-9389 (Long Win, Taiwan, China), while the through-plane ($k_\perp$) and in-plane ($k_{//}$) thermal conductivity, k, were calculated from the equation as follows:

$$k = \alpha \times \rho \times c \quad (2)$$

where α is the thermal diffusivity recorded by an LFA 467 laser-flash diffusivity instrument (NETZSCH, Hanau, Germany), ρ is the bulk density (1.58 g cm^{-3}) determined using an electronic density balance, c is the specific heat capacity (1.15 J g^{-1} °C^{-1}) detected by a 200 F3 differential scanning calorimetry (NETZSCH, Hanau, Germany) at a heating rate of 10 °C min^{-1}.

3. Results and discussion

3.1. Surface modification of h-BN

To improve surface activity of h-BN, a new non-covalent modifier DMY was utilized to functionalize the h-BN micro-platelets (Fig. 2a–b). Subsequently, the functional groups on the surface of h-BN@DMY were detected by FTIR (Fig. S1a), which presents characteristic peaks at 3426, 1655 and 1099 cm^{-1}, corresponding to –OH, C=O and C–O–C stretching vibration peaks of DMY [25], respectively. Moreover, the absorptions at 1381 and 816 cm^{-1} belonging to B–N stretching and B–N–B bending of

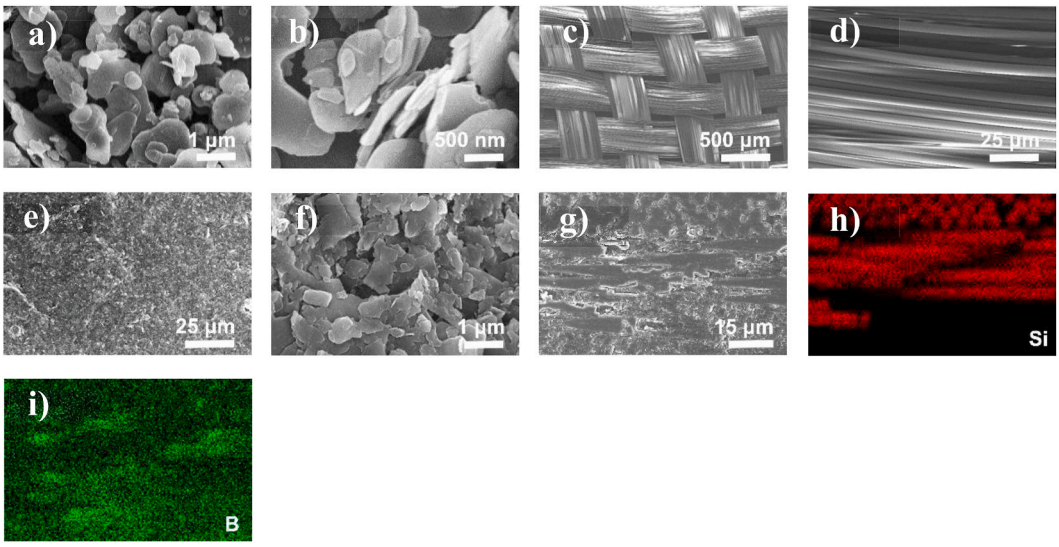

Fig. 2. SEM images of (a, b) h-BN@DMY, and surfaces of (c, d) original GFC and (e, f) GFC@1A. (g) SEM image and element mappings of (h) Si (representing glass fibers) and (i) B (representing h-BN sheets) on the cross-section of GFC@1A.

h-BN can be observed [26]. Besides, the π-bond interaction between h-BN micro-platelets and DMY was proved by UV–vis spectroscopy (Fig. S1b). For DMY, the absorption peak at about 290 nm corresponds to π-π* transition of benzoyl moieties [27]. After mixing with h-BN, the intensity of the original absorption at 290 nm decreases and a red shifted absorption appears at 323 nm, implying the existence of π-π interactions between DMY and h-BN [28]. On the other hand, the result of TGA reveals that the loading of DMY on the h-BN surface is 2.0 wt% (Fig. S1c).

Since commercial DMY may be dehydrated at elevated temperature, pretreatment at 200 °C was carried out to enhance the thermal stability of h-BN@DMY for its application in composites. As shown in Fig. S2, the heat treatment at 200 °C has no influence on the ^{1}H and ^{13}C chemical shifts of DMY, but the higher temperature treatment at 270 °C significantly alters its chemical structure. The hydrophilicity of h-BN and modified h-BN examined by contact angle tests is shown in Table S2, which demonstrates that the water contact angle of h-BN@DMY (64.80°) is greatly reduced as compared to h-BN (85.05°). Furthermore, hydrophilicity of h-BN@DMY-200 (65.26°) remains nearly unchanged. Nevertheless, the water contact angle of h-BN@DMY-270 increases to 75.64°.

3.2. Construction of in-plane thermal conductive pathways on GFC surfaces and the related laminates

For constructing in-plane thermal conductive pathways in the composite, the GFC was homogeneously coated with layers of thermally conductive film composed of high content h-BN@DMY-200 and ACR/epoxy polymer binder. The high molecular weight ACR can compulsively connect h-BN@DMY-200 sheets by means of the intermolecular forces (i.e. hydrogen bonding and van der Waals interaction) between the functional groups (e.g., carbonyl and carboxyl) of the polymer chains and the hydroxyl of DMY absorbed on the h-BN surfaces. As verified in Fig. S3, due to the intermolecular hydrogen bonds formed between DMY and ACR, the absorption peak of hydroxyl groups of the DMY/ACR mixture shifts to lower wavenumber (3323 cm^{-1}) [29,30]. Meanwhile, a new absorption assigned to hydrogen bonded carbonyl groups of ACR appears at 1700 cm^{-1} [31,32]. It no doubt benefits the adhesion at the interface. Moreover, the chains of epoxy also contain a few hydroxyl groups, which may form hydrogen bonds with ACR (Fig. 1a), so as to improve the compatibility.

The surface morphologies of GFC before and after coating are observed by SEM. As shown in Fig. 2c–d, the original GFC presents regular warp and weft structure, as well as smooth surfaces of the single fibers. After coating with h-BN@DMY-200/ACR/epoxy mixture solution, the h-BN micron platelets are tightly stacked layer by layer along the horizontal direction on the surface of the GFC with the aid of Mayer rod (Fig. 2e–f). Moreover, the SEM images and element mappings of the cross-section of GFC@1A (Fig. 2g, h and 2i) indicate that the h-BN micron sheets are embedded in the interlayer gaps of GFC, forming heat conduction pathways across the GFC. Since the commercial GFC had already been modified by silane coupling agent KH550 (see Fig. S4, the absorption peak near 3458 cm^{-1} is ascribed to amino group), the epoxy groups in the coating could further react with the amino group to increase the interfacial adhesion.

To have deeper understanding of the influence of the coating layers and polymer binder type on the morphologies of the composite laminates, SEM images and EDS mappings (i.e. B, Si and Br elements) of the cross-sections of GFC@xA/0EP and GFC@xP/0EP laminates are shown in Fig. 3 and Fig. S5. For the GFC with fewer layers of the ACR based coating, it can be seen from the B element distribution that there is a layer of pure epoxy between two GFC (Fig. 3b–f). On the contrary, for h-BN@DMY-200/PVDF/epoxy coated GFC, no obvious epoxy layer between the GFC is observed (Fig. 3d–h). The results imply that the ACR with a large number of polar groups has good wetting with epoxy, while the interaction between PVDF and epoxy is weaker, which makes it difficult for the pure epoxy to adhere on the surface of PVDF coated GFC during Mayer rod coating. In the case of the composites with ACR binder, the pure epoxy layer disappears with increasing the coating times to 3–5 (Fig. 3j, n and 3r). This is mainly attributed to the increased content of the inorganic h-BN micron platelets (Fig. 4a), which deteriorates the surface wettability of the modified GFC. But still no cracks or defects are observed as reflected by the SEM images. With regard to the material with PVDF binder, however, voids and defects can be seen in both GFC layers and epoxy matrix (Fig. 3s and t) when the coating time rises to 5.

The above results prove that ACR has superior interaction with epoxy matrix as compared with the common binder PVDF, which must be conducive for the preparation of composite with better performance. The deduction is confirmed by the contact angle measurements (Table S3), which imply that the surface properties of epoxy and acrylate copolymers are closer.

Fig. 4a shows the dependences of BN content of GFC@xA/0EP and GFC@xP/0EP composite laminates on the coating times, which are estimated from the TGA analysis in Figs. S6a and S6b according to

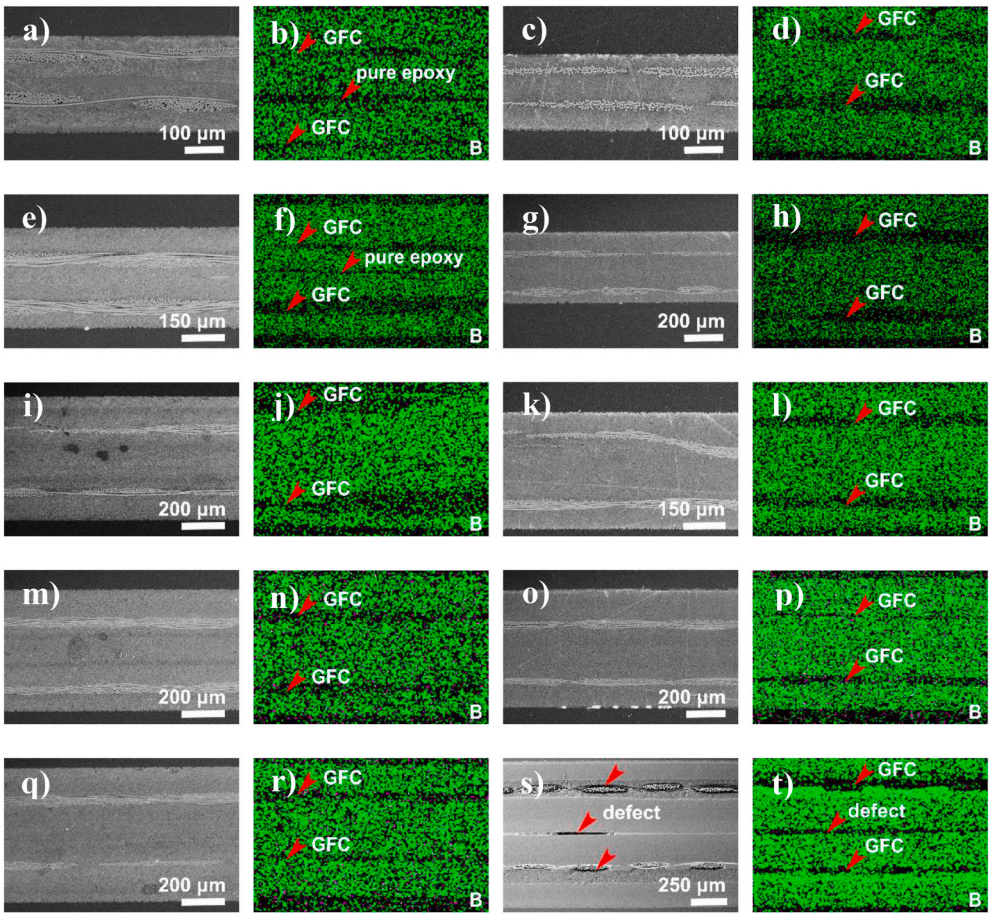

Fig. 3. SEM images and the B element mapping of the cross-sections of (a, b) GFC@1A/0EP, (c, d) GFC@1P/0EP, (e, f) GFC@2A/0EP, (g, h) GFC@2P/0EP, (i, j) GFC@3A/0EP, (k, l) GFC@3P/0EP, (m, n) GFC@4A/0EP, (o, p) GFC@4P/0EP, (q, r) GFC@5A/0EP, and (s, t) GFC@5P/0EP.

Equation (1). As expected, the BN content increases with a rise of coating times (i.e. coating layers). For the laminates derived from different polymer binders, the BN contents are similar under the same conditions, which are about 17 wt%, 30 wt%, 40 wt%, 45 wt% and 50 wt% for the coating varying from 1 to 5 layers, respectively. When the BN content increases from 17 wt% to 30 wt%, the k_o value rapidly increases from 0.34 W m^{-1} K^{-1} to 1.03 W m^{-1} K^{-1}, which implies that continuous thermally conductive networks are formed under the circumstances [33]. Generally, the k_o values significantly increase with the coating layers due to the increase of BN content (Fig. 4a), while the mechanical properties drop drastically (Fig. 4b, Fig. S6e, Fig. S6f). For example, k_o value of GFC/0EP without the thermally conducting fillers is only 0.26 W m^{-1} K^{-1}, however, that of GFC@5A/0EP increases to 1.25 W m^{-1} K^{-1} after coating 5 layers of h-BN@DMY-200/ACR/epoxy on GFC. Meantime, the tensile strength and elongation at break of GFC/0EP without the thermally conducting fillers decrease from 113.6 MPa to 2.63% to 46.2 MPa and 0.96%, respectively, due to the increase of interfacial defects between the polymer binders and h-BN micron sheets [19]. As revealed in Fig. 4a, b and Table S4, the GFC@xA/0EP laminates possess higher k_o and mechanical properties than those of GFC@xP/0EP with the same coating layers, which must be due to the improved compatibility and fewer defects between ACR and epoxy matrix (Fig. 3).

In addition, the impact of the thermally conductive coating layers on thermal properties and stability of the composite laminates is studied. As shown in Fig. 4c–4f, the glass transition temperatures, T_g, of the laminates composed of GFC and pure epoxy are 134.2 and 149.6 °C, respectively. Table S4 further shows that the T_g values of GFC@xA/0EP and GFC@xP/0EP composites (123.0–132.6 °C measured by DSC, and 113.7–143.9 °C measured by DMA) decrease after the incorporation of the modified h-BN and polymer binder. The competition between the following two opposite factors should account for the variation. With increasing the number of the coating layers, the increased h-BN microsheets would restrain more epoxy molecules, and hence hinder the movement of the chain segments and result in the raised T_g [34,35]. On the contrary, the increase of ACR and PVDF binder content with lower T_g (i.e. ~10 °C and −39 °C, respectively, Fig. S7) would decrease T_g of the system. Furthermore, incorporation of h-BN fillers reduces the heights of the tan δ peaks (Fig. 4e–f) by restricting the movement of epoxy molecules and increases the initial storage moduli (Figs. S6c and S6d) [36,37]. The width of the tan δ peak becomes broader than that of the GFC/0EP, suggesting that the modified h-BN fillers may have brought in various kinds of relaxation modes to the molecular chains [35,38]. Fig. S6a and Fig. S6b also proves that thermo-oxidative decomposition behaviors of the GFC@xA/0EP and GFC@xP/0EP laminates resemble that of the pure GFC/0EP. The onset weight loss temperature, T_i, shifts to higher temperature region (with an increment of 1.1–14.6 °C, Table S4), implying that the thermo-oxidative stability of epoxy is slightly improved with the increase of BN content.

3.3. *Construction of through-plane thermal conductive pathways in epoxy matrix and the corresponding composite laminates*

For achieving the designed composite laminates with decent TC and mechanical properties, the GFC@1A with only one layer of the thermally conductive coating containing ACR as the binder is used for construction of through-plane thermal conductive pathways. When the GFC@1A is immersed by the mixture solution of h-BN@DMY-200/epoxy, the h-BN sheets on GFC/1A should be able to closely contact and

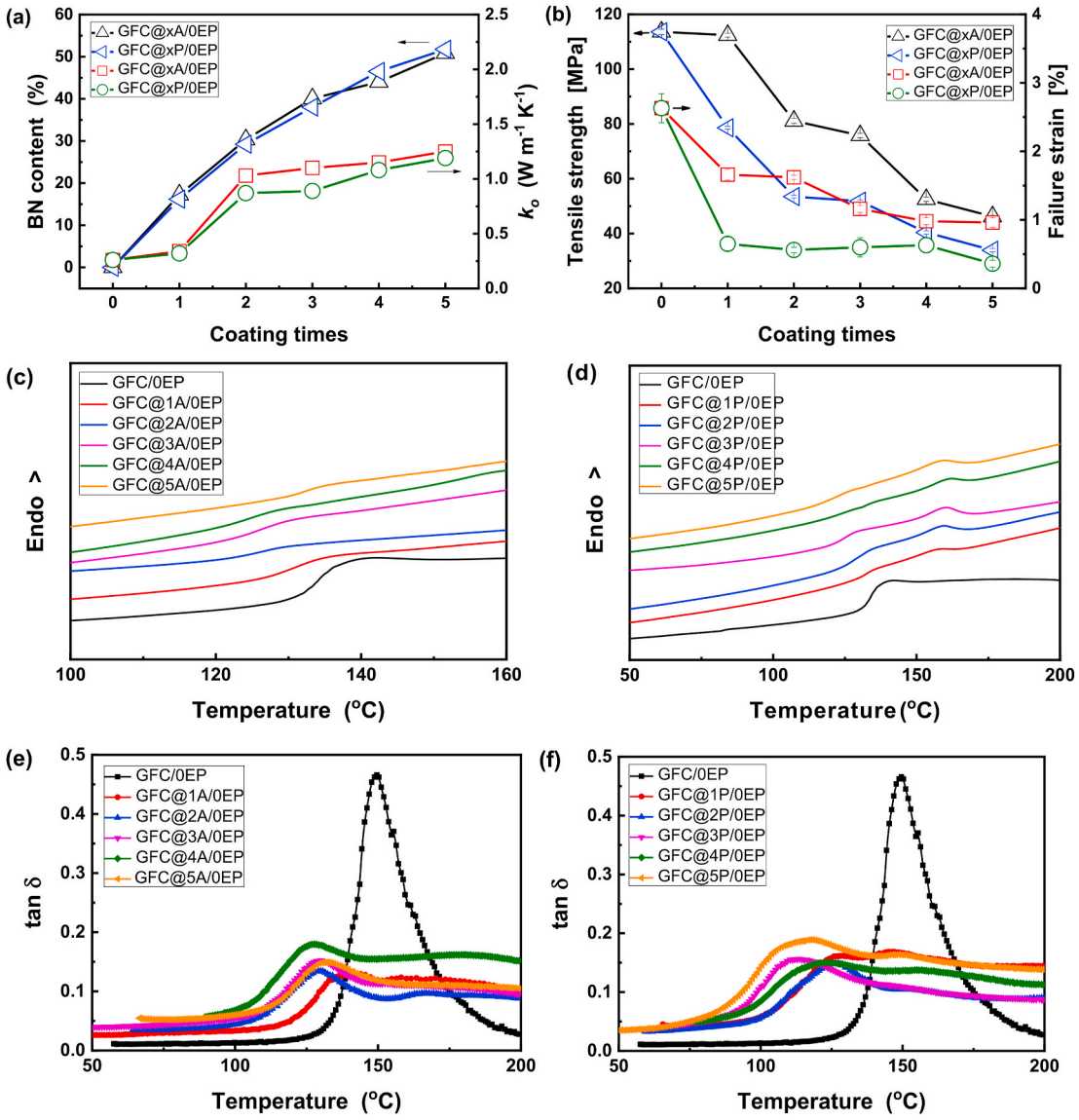

Fig. 4. (a) BN content, k_o and (b) mechanical properties of GFC@xA/0EP and GFC@xP/0EP composites as a function of coating times. DSC curves and tan δ curves of (c, e) GFC@xA/0EP and (d, f) GFC@xP/0EP composites.

overlap with the h-BN sheets in the epoxy matrix.

The microstructure morphologies of the cross-sections of the GFC@1A/yEP composites are examined by SEM and EDS mapping (Fig. 5 and Fig. S8). When the contents of h-BN sheets in the epoxy matrix are 5 wt% and 10 wt%, obvious epoxy matrix layer could be observed due to the lower content of the fillers in comparation with that of GFC@1A (i.e. 17.2 wt%). As the amount of h-BN sheets increases to 15 wt% and 20 wt%, the boundary between GFC@1A and epoxy matrix gradually becomes vague. Furthermore, the enlarged views of the interfacial region between GFC@1A and epoxy matrix in the GFC@1A/20EP laminate (Fig. 5g, circled regions I, II and III in red) indicate that the h-BN micron-sheets are tightly bonded to the surface of GFC (Fig. 5i), while the distribution of h-BN in the matrix is relative sparse (Fig. 5j and k). The observation is consistent with the h-BN content in the epoxy matrix layer estimated from TGA (i.e. 29.6–17.2 = 12.4 wt%, where 29.6, 17.2 and 12.4 wt% are the contents of h-BN in GFC@1A/20EP laminate, GFC@1A, and epoxy matrix layer, respectively, refer to Table S4). Besides, although the EDS mappings seem to show that the GFC has lower content of B (e.g., Fig. 5h) and Br (e.g., Fig. S8g) because the glass fibers have blocked the vision, it doesn't mean that this GFC region adversely affects the vertical thermal conductivity of the material. The SEM and element mapping images of GFC@1A/20EP with higher resolution (Fig. 5l~5°) demonstrate that a large number of h-BN sheets can penetrate into the internal gaps of GFC. Nevertheless, there are still a few unfilled micro-voids (Fig. S10a) due to the imperfect wetting between GFC and h-BN filled epoxy.

Interestingly, the h-BN sheets are found to be preferentially oriented in the composite. In general, the XRD intensity ratio between (002) and (100) lattice planes reflects the orientation degree of boron nitride sheets [40], which is hard to be judged from SEM images (Figs. S10b and S10c). According to this criterion, it is seen from (Fig. 6d) that although the orientation degree of h-BN within epoxy (i.e. GFC@1A/20EP, $I_{(002)}/I_{(110)} = 72$) is smaller than that of the thermally conductive layer on the GFC surface (i.e. GFC@1A, $I_{(002)}/I_{(110)} = 94$), it is still much higher than that of the h-BN powders ($I_{(002)}/I_{(110)} = 8$). Clearly, the h-BN micron sheets in the thermally conductive layers and epoxy matrix tend to align along the horizontal direction under the joint action of Mayer rod, Teflon scraper and hot pressing [38,39].

Fig. 6a displays that k_o values of GFC@1A/yEP composites are improved with the increasing of BN loading in epoxy matrix. The total BN content of the composite laminates ranges from 17.2 to 29.6 wt% as calculated by TGA (Fig. S9a) and Equation (1). The gradual

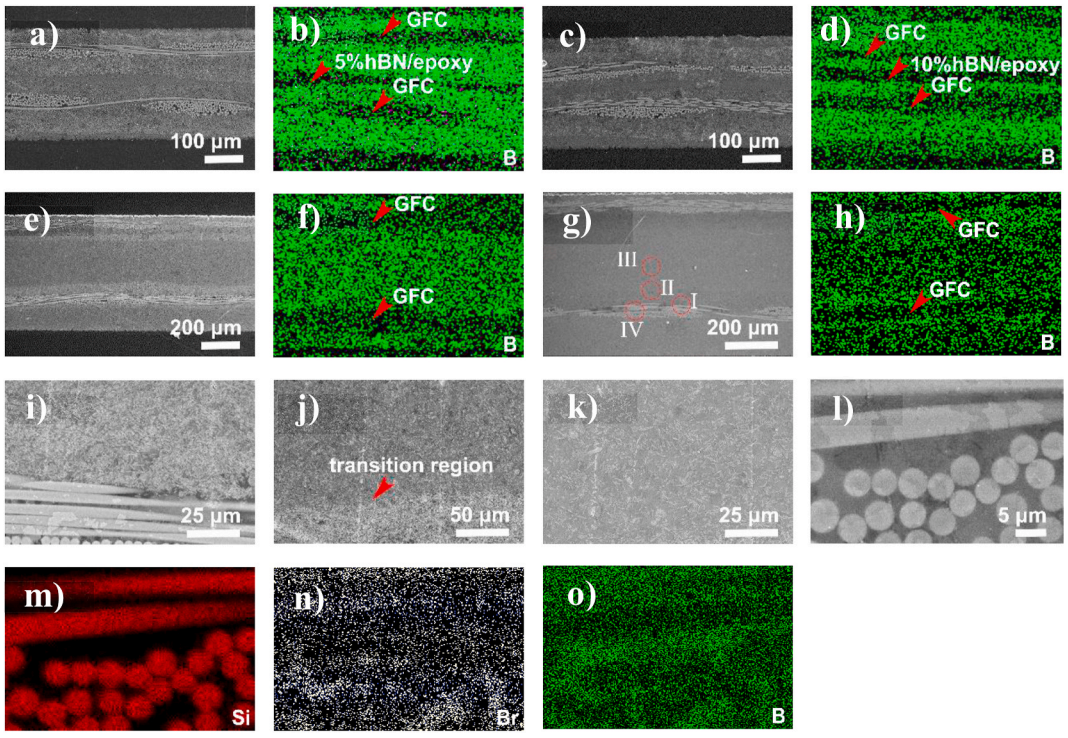

Fig. 5. SEM images and B element mappings of the cross-sections of (a, b) GFC@1A/5EP, (c, d) GFC@1A/10EP, (e, f) GFC@1A/15EP, and (g, h) GFC@1A/20EP. (i, j, k, l) SEM images of the enlarged views of the circled regions I, II, III and IV in red in (g). I: The interfacial region between GFC and h-BN@DMY-200/ACR/epoxy coating. II: The interfacial region between h-BN@DMY-200/ACR/epoxy coating and 20 wt% h-BN@DMY-200/epoxy matrix. III: Morphology of h-BN@DMY-200/epoxy matrix. IV: The interlayer region of GFC. (m, n, o) Element mappings of Si (representing glass fibers), Br (representing epoxy) and B (representing h-BN sheets) in (l). (For interpretation of the references to colour in this figure legend, the reader is referred to the Web version of this article.)

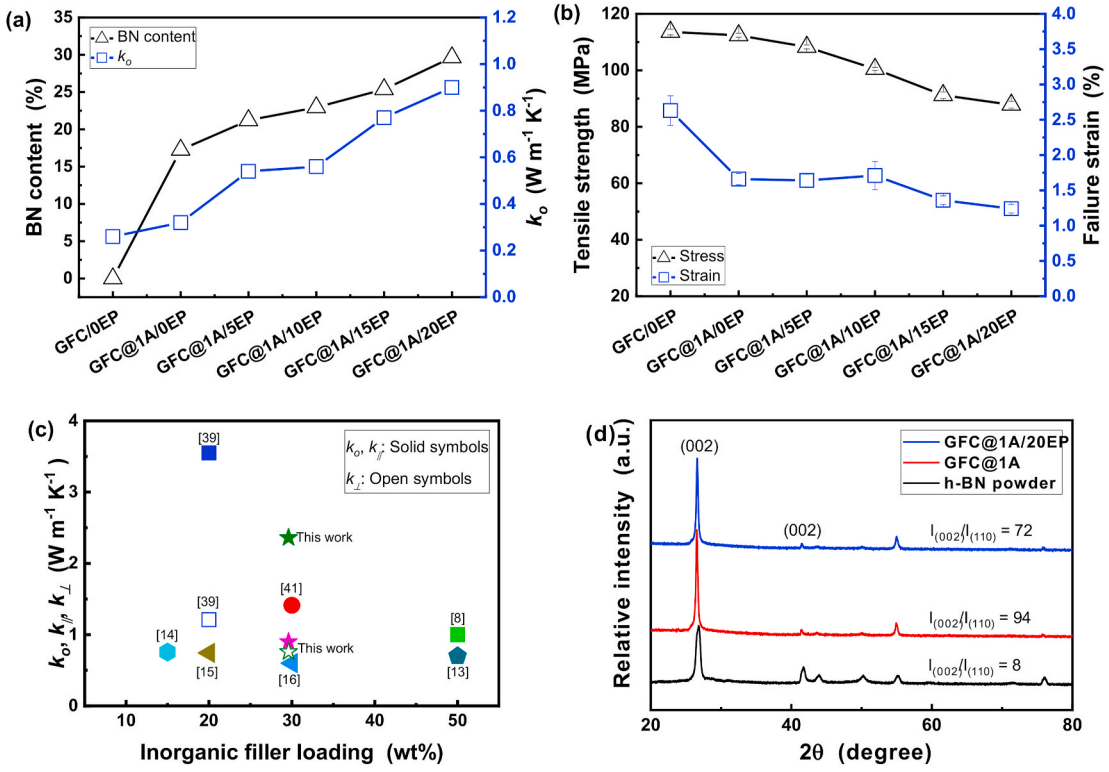

Fig. 6. (a) BN content, k_o, and (b) mechanical properties of GFC@1A/yEP composites. (c) Dependences of TC of the glass fiber cloth reinforced polymer composites on inorganic fillers content reported in literature in comparison with the results of this work. (d) XRD spectra of h-BN powder, GFC@1A, and GFC@1A/20EP.

improvement of thermal conductive pathways effectively reduces the interfacial phonon scattering and thermal resistance [6]. Consequently, the k_o of GFC@1A/20EP detected by steady state method is increased by 3.5 times (i.e. 0.90 W m^{-1} K^{-1}, Table S4) of the original value (0.26 W m^{-1} K^{-1}). Meanwhile, the $k_{//}$ and $k_{\perp}$ values measured by LFA approach are 2.36 and 0.76 W m^{-1} K^{-1}, respectively.

To understand the main factors responsible for improving TC of the composite, two epoxy composites containing the same mass fraction of h-BN@DMY as that of GFC@1A/20EP (i.e. 29.6 wt%) but excluding GFC were fabricated as reference materials by solution casting (i.e. Epoxy/h-BN-C) and Mayer rod coating (i.e. Epoxy/h-BN-M), respectively. The in-plane and through-plane thermal conductivities of the former are detected to be 0.44 and 0.38 W m^{-1} K^{-1} (Table S5), while those of the latter are 1.38 and 0.49 W m^{-1} K^{-1} (Table S5), which are all lower than the corresponding properties of GFC@1A/20EP composite. It is thus known the important contributions of the well designed in-plane and through-plane thermally conductive pathways, and the processing-induced orientation of h-BN sheets (Fig. 6d) during fabrication as well. The efficient in-plane thermally conductive pathways are constructed by introducing thermally conductive layer from high h-BN concentration epoxy based coating (mass ratio of h-BN to resin = 4.5/1) onto GFC with Mayer rod. In the meantime, a few h-BN sheets are squeezed into the interstitial gaps of the glass fiber cloth, forming heat conduction paths across the GFC and eventually favoring through-plane thermal conduction of the composite in cooperation with the lower h-BN concentration (20 wt%) epoxy matrix. Moreover, the surface modification of h-BN sheets using DMY also exerts positive effect. Table S5 shows that the control composite, GFC@1A/20EP-ref, which contains 29.6 wt % unmodified h-BN sheets, has lower thermal conductivities (2.1 and 0.66 W m^{-1} K^{-1}) and tensile strength (75.1 MPa) than GFC@1A/20EP owing to the relatively poor dispersion of the unmodified h-BN sheets and higher interface thermal resistance between h-BN platelets and epoxy.

The thermal conductivities obtained in this work is close to or even higher than those of the previous reported GFC/epoxy laminates (Fig. 6c, Table S6) at lower filler content [8,14,15,36]. It is worth noting that the fillers like spherical boron nitride (s-BN) and Si_3N_4 [41,43] are much more expensive than h-BN, so that they are difficult to be used in industrial production on a large scale.

On the other hand, the thermal conductivities of commercially thermally conductive glass fiber/epoxy laminates are generally around 1–1.5 W m^{-1} K^{-1} (Table S7), which means that the composites developed in this work can meet the actual heat dissipation requirements. Besides, electrical insulation is also important for practical application of PCBs as mentioned in the Introduction. The volume resistivity and surface resistivity of GFC@1A/20EP are detected to be 9.69×10^{16} Ω cm and 8.86×10^{15} Ω, respectively, exhibiting superior electrically insulating performance like other thermally conductive insulating composites [31,44–46].

It has been reported that a small amount of h-BN fillers (e.g., 2–3 wt %) can improve the mechanical strength of epoxy resin due to the effective absorption of fracture energy and prevention of crack propagation by h-BN sheets [19]. While in the condition of higher filler loading, the increase of interfacial defects between polymer matrix and fillers may become the main fracture source under external force, and lead to attenuation of mechanical strength [19,42]. Owing to the fact that the majority of the h-BN micro-sheets are entrapped in the GFC zones, which helps to relieve stress concentration in the matrix to a certain degree, however, the negative influence of high particulate fillers loading on mechanical properties of the composite is minimized. As a result, 78.1% (i.e. 87.8 MPa) and 74.7% (i.e. 1.24%) of the original tensile strength and elongation at break can be maintained even for GFC@1A/20EP (Fig. 6b), in spite of the fact the overall mechanical properties decline with increasing additives. Not only the tensile strength is comparable to those of the reported glass fiber/epoxy composite laminates with even higher glass fiber content (e.g., ~40 wt%) [47–50], but also the retention of tensile strength at the similar thermally conductive fillers content is higher than the reported values (about 64.3–67.0%) [19,42].

4. Conclusions

To develop inexpensive non-covalent functionalization method for the inert surface of h-BN, dihydromyricetin is used to increase surface polarity through the large π-bond conjugate interaction. The resultant h-BN@DMY-200 μm platelets exhibit good hydrophilicity and compatibility with the epoxy matrix. Afterwards, a facile two-step coating method for fabricating highly thermally conductive GFREP is applied with h-BN@DMY-200 as the thermally conductive fillers. The thermally conductive coating on GFC surface can effectively construct in-plane thermal conductive paths, and reduce the interfacial heat resistance between GFC and epoxy matrix as well. As compared to PVDF binder, ACR shows better compatibility and fewer defects between the thermally conductive coating and epoxy matrix. After infiltration of the epoxy resin containing fewer h-BN@DMY-200, through-plane thermally conductive pathways are formed. The composite made from only one layer of h-BN@DMY-200/ACR/epoxy coating and the epoxy matrix with 20 wt% h-BN@DMY-200 shows excellent $k_{//}$ and $k_{\perp}$, which are 2.36 and 0.76 W m^{-1} K^{-1}, respectively. Meanwhile, 78.1% (i.e. 87.8 MPa) and 74.7% (i.e. 1.24%) of the original tensile strength and elongation at break can be maintained under the circumstances because the majority of the h-BN micro-sheets are entrapped in the fiber-rich zone.

CRediT authorship contribution statement

Hua Xiao: Data curation, Investigation. **Fang Chen:** Investigation. **Ze Ping Zhang:** Writing – original draft, Writing – review & editing, Visualization, Funding acquisition. **Min Zhi Rong:** Methodology, Writing – review & editing, Funding acquisition. **Ming Qiu Zhang:** Methodology, Writing – review & editing, Supervision, Funding acquisition.

Declaration of competing interest

The authors declare that they have no known competing financial interests or personal relationships that could have appeared to influence the work reported in this paper.

Acknowledgements

This work was supported by National Natural Science Foundation of China, China (No. 52033011, 51873235, 51773229 and 51973237), Natural Science Foundation of Guangdong Province, China (Grant: 2019B1515120038, 2020A1515011276, 2018B030311017) and Science and Technology Planning Project of Guangdong Province, China (Grant: 2020B010179001).

Appendix A. Supplementary data

Supplementary data to this article can be found online at https://doi.org/10.1016/j.compositesb.2021.108770.

References

[1] Kim YH, Lim YW, Kim YH, Bae BS. Thermally stable siloxane hybrid matrix with low dielectric loss for copper-clad laminates for high-frequency applications. ACS Appl Mater Interfaces 2016;8:8335–40.
[2] Yang X, Zhu J, Yang D, Zhang J, Guo Y, Zhong X, Kong J, Gu J. High-efficiency improvement of thermal conductivities for epoxy composites from synthesized liquid crystal epoxy followed by doping BN fillers. Compos B Eng 2020;185:107784.
[3] Yang X, Zhong X, Zhang J, Gu J. Intrinsic high thermal conductive liquid crystal epoxy film simultaneously combining with excellent intrinsic self-healing performance. J Mater Sci Technol 2021;68:209–15.

[4] Ruan K, Shi X, Guo Y, Gu J. Interfacial thermal resistance in thermally conductive polymer composites: a review. Compos Commun 2020;22:100518.
[5] Zhou W, Liang G, Fang H, Ren P, Yang J. Advance in the research of high performance copper clad laminate based on resin matrix. Eng Plast Appl 2004;32:71–4.
[6] Zhang R, Shi X, Tang L, Liu Z, Zhang J, Guo Y, Gu J. Thermally conductive and insulating epoxy composites by synchronously incorporating Si-sol functionalized glass fibers and boron nitride fillers. Chin J Polym Sci 2020;8:730–9.
[7] Assael MJ, Antoniadis KD, Metaxa IN, Tzetzis D. Measurements on the enhancement of the thermal conductivity of an epoxy resin when reinforced with glass fiber and carbon multiwalled nanotubes. J Chem Eng Data 2008;54:2365–70.
[8] Ge M, Zhang J, Zhao C, Lu C, Du G. Effect of hexagonal boron nitride on the thermal and dielectric properties of polyphenylene ether resin for high-frequency copper clad laminates. Mater Des 2019;182:108028.
[9] Wang Z, Liu W, Liu Y, Ren Y, Li Y, Zhou L, Xu J, Lei J, Li Z. Highly thermal conductive, anisotropically heat-transferred, mechanically flexible composite film by assembly of boron nitride nanosheets for thermal management. Compos B Eng 2020;180:107569.
[10] Fu C, Yan C, Ren L, Zeng X, Du G, Sun R. Improving thermal conductivity through welding boron nitride nanosheets onto silver nanowires via silver nanoparticles. Compos Sci Technol 2019;177:118–26.
[11] Leung SN. Thermally conductive polymer composites and nanocomposites: processing structure-property relationships. Compos B Eng 2018;150:78–92.
[12] Zhang X, Wu K, Liu Y, Yu B, Zhang Q, Chen F, Fu Q. Preparation of highly thermally conductive but electrically insulating composites by constructing a segregated double network in polymer composites. Compos Sci Technol 2019;175:135–42.
[13] Yao Y, Zeng X, Guo K, Sun R, Xu JB. The effect of interfacial state on the thermal conductivity of functionalized Al_2O_3 filled glass fibers reinforced polymer composites. Compos Part A: Appl S 2015;69:49–55.
[14] Qi H, Qi S, Li M, Lu H. Preparation and properties of epoxy resin/glass fiber/BN high thermal conductive composites. Adhes Chin 2010;31:52–5.
[15] Wu J, Qi S, Li J. Preparation of epoxy resin/glass cloth/BN thermal conductive and insulating composites. Adhes Chin 2011;32:68–70.
[16] Xie F, Qi S, Li J. Study on preparation and property of polyimide modified epoxy resins/glass fiber thermally conductive composite filled with Al_2O_3 particles. China Plast 2013;27:57–61.
[17] Kim K, Kim J. Fabrication of thermally conductive composite with surface modified boron nitride by epoxy wetting method. Ceram Int 2014;40:5181–9.
[18] Fu L, Wang T, Yu J, Dai W, Sun H, Liu Z, Sun R, Jiang N, Yu A, Lin CT. An ultrathin high-performance heat spreader fabricated with hydroxylated boron nitride nanosheets. 2D Mater 2017;4:025047.
[19] Hou J, Li G, Yang N, Qin L, Grami ME, Zhang Q, Wang N, Qu X. Preparation and characterization of surface modified boron nitride epoxy composites with enhanced thermal conductivity. RSC Adv 2014;4:44282–90.
[20] Chejanovsky N, Rezai M, Paolucci F, Kim Y, Rendler T, Rouabeh W, de Oliveira FF, Herlinger P, Denisenko A, Yang S, Gerhardt I, Finkler A, Smet JH, Wrachtrup J. Structural attributes and photo-dynamics of visible spectrum quantum emitters in hexagonal boron nitride. Nano Lett 2016;16:7037–45.
[21] Jiang F, Cui S, Rungnim C, Song N, Ding P. The control of a dual-cross-linked boron nitride framework and the optimized design of the thermal conductive network for its thermoresponsive polymeric composites. Chem Mater 2019;31:7686–95.
[22] Zeng X, Ye L, Yu S, Li H, Sun R, Xu J, Wong CP. Artificial nacre-like papers based on noncovalent functionalized boron nitride nanosheets with excellent mechanical and thermally conductive properties. Nanoscale 2015;7:6774–81.
[23] Shen H, Guo J, Wang H, Zhao N, Xu J. Bioinspired modification of h-BN for high thermal conductive composite films with aligned structure. ACS Appl Mater Interfaces 2015;7:5701–8.
[24] Yu J, Huang X, Wu C, Wu X, Wang G, Jiang P. Interfacial modification of boron nitride nanoplatelets for epoxy composites with improved thermal properties. Polymer 2012;53:471–80.
[25] Guo Q, Guo Q, Yuan J, Zeng J. Biosynthesis of gold nanoparticles using a kind of flavonol: Dihydromyricetin. Colloids Surf, A 2014;441:127–32.
[26] Shi Y, Hamsen C, Jia X, Kim KK, Reina A, Hofmann M, Hsu AL, Zhang K, Li H, Juang ZY, Dresselhaus MS, Li L, Kong J. Synthesis of few-layer hexagonal boron nitride thin film by chemical vapor deposition. Nano Lett 2010;10:4134–9.
[27] Zsila F, Bikádi Z, Simonyi M. Probing the binding of the flavonoid, quercetin to human serum albumin by circular dichroism, electronic absorption spectroscopy and molecular modelling methods. Biochem Pharmacol 2003;65:447–56.
[28] Ye TX, Ye SL, Chen DM, Chen QA, Qiu B, Chen X. Spectroscopic characterization of tetracationic porphyrins and their noncovalent functionalization with graphene. Spectrochim Acta 2012;86:467–71.
[29] Kim GH, Lee D, Shanker A, Shao L, Kwon MS, Gidley D, Kim J, Pipe KP. High thermal conductivity in amorphous polymer blends by engineered interchain interactions. Nat Mater 2015;14:295–300.
[30] Jiang F, Cui S, Song N, Shi L, Ding P. Hydrogen bond regulated boron nitride network structures for improved thermal conductive property of polyamide-imide composites. ACS Appl Mater Interfaces 2018;10:16812–21.
[31] Jo WH, Cruz CA, Paul DR. FTIR investigation of interactions in blends of PMMA with a styrene/acrylic acid copolymer and their analogs. J Polym Sci, Polym Phys Ed 1989;27:1057–76.
[32] Kuo SW, Huang CF, Chang FC. Study of hydrogen-bonding strength in poly (ε-caprolactone) blends by DSC and FTIR. J Polym Sci, Polym Phys Ed 2001;39:1348–59.
[33] Li M, Wang M, Hou X, Zhan Z, Wang H, Fu H, Lin C, Fu L, Jiang N, Yu J. Highly thermal conductive and electrical insulating polymer composites with boron nitride. Compos B Eng 2020;184:107746.
[34] Li TL, Hsu SLC. Preparation and properties of thermally conductive photosensitive polyimide/boron nitride nanocomposites. J Appl Polym Sci 2011;121:916–22.
[35] Li TL, Hsu SLC. Enhanced thermal conductivity of polyimide films via a hybrid of micro- and nano-sized boron nitride. J Phys Chem B 2010;114:6825–9.
[36] Kim K, Kim M, Hwang Y, Kim J. Chemically modified boron nitride-epoxy terminated dimethylsiloxane composite for improving the thermal conductivity. Ceram Int 2014;40:2047–56.
[37] Zhang Y, Park M, Park SJ. Implication of thermally conductive nanodiamond-interspersed graphite nanoplatelet hybrids in thermoset composites with superior thermal management capability. Sci Rep 2019;9:2893.
[38] Dong S, Gauvin R. Application of dynamic mechanical analysis for the study of the interfacial region in carbon fiber/epoxy composite materials. Polym Compos 1993;14:414–20.
[39] Yu C, Gong W, Tian W, Zhang Q, Xu Y, Lin Z, Hu M, Fan X, Yao Y. Hot-pressing induced alignment of boron nitride in polyurethane for composite films with thermal conductivity over 50 Wm^{-1} K^{-1}. Compos Sci Technol 2018;160:199–207.
[40] Wang H, Ding D, Liu Q, Chen Y, Zhang Q. Highly anisotropic thermally conductive polyimide composites via the alignment of boron nitride platelets. Compos B Eng 2019;158:311–8.
[41] Tang L, He M, Na X, Guan X, Zhang R, Zhang J, Gu J. Functionalized glass fibers cloth/spherical BN fillers/epoxy laminated composites with excellent thermal conductivities and electrical insulation properties. Compos Commun 2019;16:5–10.
[42] Gong Y, Zhou W, Kou Y, Xu L, Wu H, Zhao W. Heat conductive h-BN/CTPB/epoxy with enhanced dielectric properties for potential high-voltage applications. High Volt 2017;2:172–8.
[43] Zhang J, Qi S. Preparation and properties of silicon nitride/glass fiber/epoxy composites. Polym Compos 2014;35:1338–42.
[44] Wang Y, Zhang X, Ding X, Zhang P, Shu M, Zhang Q, Gong Y, Zheng K, Tian X. Imidization-induced carbon nitride nanosheets orientation towards highly thermally conductive polyimide film with superior flexibility and electrical insulation. Compos B Eng 2020;199:108267.
[45] Chen J, Huang X, Sun B, Jiang P. Highly thermally conductive yet electrically insulating polymer/boron nitride nanosheets nanocomposite films for improved thermal management capability. ACS Nano 2019;13:337–45.
[46] Shi X, Zhang R, Ruan K, Ma T, Guo Y, Gu J. Improvement of thermal conductivities and simulation model for glass fabrics reinforced epoxy laminated composites via introducing hetero-structured BNN-30@BNNS fillers. J Mater Sci Technol 2021. https://doi.org/10.1016/j.jmst.2021.01.018.
[47] Seretisa GV, Nitodas SF, Mimigianni PD, Kouzilos GN, Manolakos DE, Provatidis CG. On the post-curing of graphene nanoplatelets reinforced hand lay-up glass fabric/epoxy nanocomposites. Compos B Eng 2018;140:133–8.
[48] Seretisa GV, Polyzou AK, Manolakos DE, Provatidis CG. Tensile performance of graphene nanoplatelets/glass fabric/epoxy nanocomposite laminae. Procedia Struct Integr 2018;10:249–56.
[49] Elkhouly HI, Abdel-Magied RK, Aly MF. An investigation of date palm seed as effective filler material of glass–epoxy composites using optimization techniques. Polym Polym Compos 2020;28:541–53.
[50] Li C, Guo K, Zeng X, Zhu D, Sun R. Preparation and properties of liquid crystal epoxy/boron nitride nanosheet/glass fiber three–phase composites. J Integr Technol 2019;8:45–53.